Transient Elastic Waves in a Transversely Isotropic Plate

Richard L. Weaver†, Wolfgang Sachse‡ and Kwang Yul Kim‡

† Department of Theoretical and Applied Mechanics
University of Illinois at Urbana-Champaign; Urbana, Illinois – 61801

‡ Department of Theoretical and Applied Mechanics
Cornell University; Ithaca, New York – 14853–1503

ABSTRACT

The elastodynamic response of a thick plate, with the axis of transverse isotropy normal to the plate surface, is calculated by double numerical inverse transforms, a method particularly well suited for calculations of responses in the near field of layered structures. Applications of these calculations include *point-source/point–receiver* ultrasonics, quantitative acoustic emission measurements, and seismology. The singularities of the integrand are eliminated by the introduction of a small, but non–zero, imaginary part to the frequency. We discuss issues of numerical efficiency and accuracy in the evaluation of the resulting integrals. The method can be generalized to calculate the responses in materials of more general symmetry, in viscoelastic materials and to include the effects of finite aperture sources and receivers. The calculated responses are compared to those measured in a single crystal specimen of zinc.

I. Introduction

Ultrasonic measurements which rely on elastic waves propagating through a material can provide an ideal means for determining the macroscopic properties of the material or for detecting flaws and inhomogeneities. The focus of much research over the past decade has been on the development of quantitative active ultrasonic and passive acoustic emission (AE) techniques. The use of ultrasound for non–destructive materials evaluation is especially appealing because of the direct connection between the characteristics of the wave propagation and the mechanical properties of a material. In contrast, passive AE techniques are attractive because they are able to monitor *in situ* the integrity of a large structure and to provide a means of investigating details of dynamic failure processes in materials.

The theory of quantitative acoustic emission represents AE signals as spatial and temporal convolutions between the unknown source functions and the elastic wave Green's functions of the specimen. Recovery of the source function, which characterizes a source of emission, is possible only

if the appropriate components of a specimen's elastic wave Green's function are known. The theory of transient wave propagation in bounded isotropic materials is now well established and has been used for the characterization of AE sources in such materials (Scruby, 1985; Kim, em et al., 1989). This approach has formed the basis of quantitative AE analysis in which the waveforms detected by well–characterized receivers are processed to recover the characteristics of the source, that is, its type, orientation and time–dependence. Similar applications in anisotropic materials have not yet been demonstrated, owing in part to the less well–developed theory for such materials.

A recent advance for obtaining ultrasonic waveform data in materials has been the development of the *point–source/point–receiver* (*PS/PR*) technique (Sachse and Kim, 1986; 1987a; 1987b; Sachse, *et al.*, 1990). The technique employs small–aperture sources and receivers and uses knowledge of the wave propagation to interpret the detected ultrasonic signals. The method exhibits a number of distinct advantages over conventional, plane–wave ultrasonic measurements. Specimen preparation requirements are reduced and broadband excitations are easily realizable. Except in special cases, a point source generates both longitudinal and shear waves in a specimen, therefore information about each of these wave modes can be extracted from a waveform. Further, since *PS/PR* signals are simultaneously propagated in a wide range of directions in a specimen, one can easily determine the direction dependence of the propagation speeds and attenuations of various wave modes. Recent application of such measurements to characterize anisotropic materials has focused on inverting ultrasonic group velocities, obtained from pulse arrival time data in signals that have propagated in non–principal directions in an uncut specimen, to obtain the matrix of elastic stiffness of the specimen material (Castagnede, *et al.*, 1991; Every, *et al.*, 1991; Every, *et al.*, 1990; Niu, 1992).

A more detailed analysis of the waveforms, and, in particular, their evolving amplitudes and shapes, however, requires that the signals be detected by a sensor of known transfer characteristics and interpreted with an understanding of the propagation of transient elastic waves in a bounded specimen. Such measurements and signal analysis can form the basis of an absolute, *quantitative* materials characterization technique in specimens of isotropic materials (Weaver, *et al.*, 1989). The same procedures should in principle also be applicable for waves in bounded, anisotropic materials, but this has not yet been demonstrated.

Essential to the development of active and passive quantitative techniques in anisotropic materials is the development of an understanding of the propagation of transient elastic waves in bounded media. This would provide a rational basis for processing and interpreting ultrasonic signals to recover the characteristics of a source of emission or to determine the propagation characteristics of the material. Preliminary work has shown that the measured dynamic Green's functions in a plate–like specimen of an anisotropic material differ significantly from those in isotropic materials (Kim, *et al.*, 1993a). A theoretical basis for calculating the transient elastic waves in a bounded anisotropic material is of great fundamental as well as practical importance. Here we take the first step, that is, the development of a method for the calculation of such waveforms in transversely isotropic plates. The method promises to be readily extendable to plates of more arbitrary anisotropy and viscous properties.

II. Elastodynamics of thick plates

The calculation of elastodynamic responses in thick plates is a generalization of "Lamb's" problem, in which the response of an isotropic half space or plate to a concentrated transient surface load may

be represented as a problem of solving the quiescent initial condition partial differential equation

$$\sigma_{ij,j} = \rho \frac{\partial^2 u_i}{\partial t^2} \quad , \tag{1}$$

where the stress tensor field is

$$\sigma_{ij} = \lambda \delta_{ij} u_{k,k} + \mu(u_{i,j} + u_{j,i}) \tag{2}$$

and traction boundary conditions are applied at the free and loaded surfaces, and traction on the other surfaces equal to the applied loads. For the case of a load $\mathbf{F}(t)$ concentrated at a point $x = y = 0$, the traction on the loaded surface at $z = h$ is

$$t_i = \sigma_{ij} n_j = F_i(t) \delta(x) \delta(y) \quad \text{at} \quad z = h \tag{3}$$

These equations may be treated by finite difference algorithms (see for example, Chang and Sun (1988) or Wu and Kuo (1990)) in which all derivatives with respect to time and space are replaced with finite difference equivalents and the resulting difference equations iterated in time. The method, in essence, numerically solves differential equations in all spatial coordinates and in time. For systems which lack translation invariance in x and y this may be the most efficient procedure.

For plates with translation invariance, however, it may be expected that the integral transform method, with attendant analytical solution of the differential equation in z, is more efficient. This is the approach taken by most researchers. The invariance of the plate under translations in time and in the coordinates x and y make it convenient to proceed by means of a Fourier, or Laplace, transform in time and a double Fourier transform in space. The result is a set of coupled, ordinary differential equations in z for the transformed fields u_i or their associated displacement potentials. In homogeneous materials, the ODE's are constant coefficient and therefore solvable in terms of linear combinations of exponentials in z. The coefficients in the linear combinations are determinable from the transformed boundary conditions. The solution is the triply–transformed response of the plate.

Because the signals are sought in either the time– or frequency–domains, the major difficulty is the need for an inversion of the transforms. At least three different methods for that inversion exist. One is *Generalized Ray Theory* (Pao and Gajewski, 1977) in which the response is written as a superposition of expressions corresponding to rays from the source to the receiver, each associated with a definite arrival time. Another method expresses the response as a sum of inverse integral transforms associated with individual branches of the dispersive guided waves (Weaver and Pao, 1982a; Vasudevan and Mal, 1985). A third method attempts a completely numerical multiple inverse integral transform (Bouchon and Aki, 1977; Weaver, *et al.*, 1989; Lih and Mal, 1992).

Generalized ray theory in which the double transform is inverted by the Cagniard method has been successfully applied to the calculation of the transient responses of isotropic half spaces (Pekeris, 1955; Knopoff, 1958), and transversely isotropic half spaces (Payton, 1983). Ray theory has also been successfully applied to the calculation of near field responses in isotropic plates (Ceranoglu and Pao, 1981; Hsu, 1985) with numerous applications to acoustic emission source characterization and to *point–source/point–receiver* ultrasonics measurements, e.g. (Scruby, 1985; Sachse and Kim, 1986). Generalized ray theory (Pao and Gajewski, 1977) expresses responses as superpositions of integrals associated with rays traveling from the source to the receiver, either directly or after one or more surface reflections, each with a well-defined arrival time. At finite

time there are a finite number of rays that contribute. In practice, however, the number of rays that contribute may be very large. The calculations are therefore cumbersome unless interest is confined to the very earliest times. Ray theory is generally not applicable to viscoelastic media (Weaver, *et al.*, 1989).

As Payton (1983) has demonstrated, responses in anisotropic media are, in principle, also decomposable into a sum of generalized rays. The calculations, however, can become very difficult to carry out because of the complexity of the folded group velocity surfaces. No one to our knowledge has attempted to carry out such calculations except for the simplest of anisotropic media: that of a transversely isotropic half space for which the symmetry axis is normal to the surface (Payton, 1983) and that of an unbounded medium of more arbitrary symmetry (Every and Kim, 1993). The response of an unbounded medium and a half space to a transient line load has been calculated by Nayfeh and Kim (1993). Van der Hijden (1987) has discussed the necessary procedures for a ray calculation in the general case of an arbitrarily layered anisotropic medium. Bedding and Willis (1980) have discussed and calculated high-frequency wave front approximations which are valid near ray arrival times.

Owing to the multitude of rays needed, ray theory is not amenable to calculation of plate responses in the far field. Nevertheless, responses in an anisotropic plate at receiver positions far from a source have been calculated by means of one analytical inverse transform done with the aid of the Cauchy residue theorem followed by a numerical inverse transform of the remaining integral (Weaver and Pao, 1982a; 1982b; Vasudevan and Mal, 1985; Santosa and Pao, 1989). The use of the Cauchy residue theorem requires the location of the poles corresponding to the Rayleigh–Lamb like waves of the plate and this can be conceptually complicated, especially in media with arbitrary layering, viscous properties and/or elastic symmetries (Nayfeh and Chimenti, 1989). Furthermore, a large number of pole locations are required for the calculation of responses with fine time resolution. This suggests that the method is not appropriate for high frequency or large bandwidth applications.

A number of researchers (Weaver, *et al.*, 1990; Xu and Mal, 1985; Lih and Mal, 1992; Kundu and Mal, 1985; Bouchon and Aki, 1977; Duprey, 1993) have discussed and implemented schemes in which the location of the Rayleigh-Lamb poles is unnecessary. In these studies, all the inversions are carried out numerically. These integrations confront one with a need to write algorithms in which the contributions from the singularities at the poles corresponding to the Rayleigh-Lamb waves are correctly evaluated. As Kundu and Mal (1985) discuss, there are a variety of techniques which have been employed to negotiate these poles. One may write an algorithm which recognizes the pole and evaluates the contribution from its vicinity by taking a numerical Cauchy principal value and supplementing it with an analytic expression for a half residue. This could be cumbersome. Mal and co–workers (Xu and Mal, 1985; Kundu and Mal, 1985; Lih and Mal, 1992) have proceeded by introducing dissipation into their materials. Except for the strong pole at low wave number and frequency, this moves the poles off the line of numerical integration. It also disperses the sharp ray arrivals. Weaver, *et al.* (1989) and Duprey (1993) have followed the method suggested by, amongst others, Bouchon and Aki (1977), of letting their frequency gain a small constant imaginary part, hence $\omega = \omega_r - \imath\delta$ where δ is small and positive. After the calculation is completed, the effect of δ is removed by multiplying responses by $\exp\{\delta t\}$. This method has the presumed disadvantage of amplifying numerical noise at late times. On the other hand it does preserve the sharp wave arrivals characteristic of non–dissipative materials. It has been demonstrated (Weaver, *et al.*, 1989; Duprey, 1993) that this approach may readily be extended to the viscoelastic case and to the use of finite aperture receivers (Duprey, 1993). Because of the presumed poor accuracy at

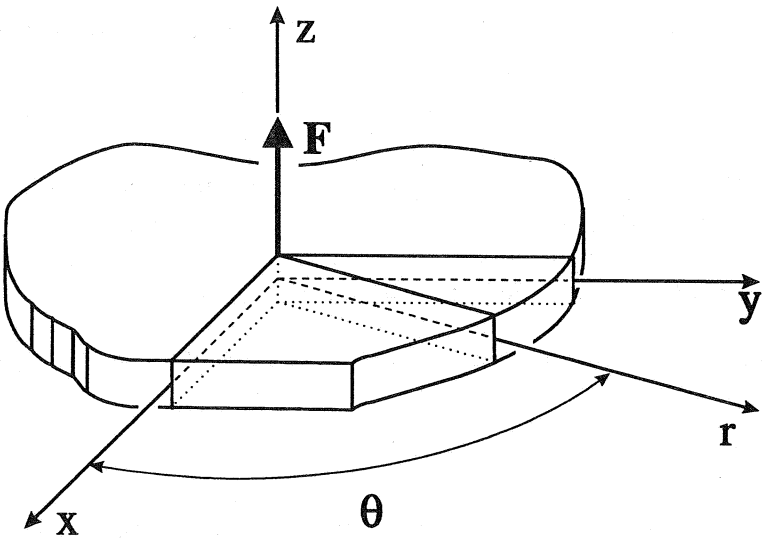

Figure 1: Geometry of the problem.

late times the method is probably most appropriate for calculation of the responses at early times and consequently for short source/receiver separations. It promises also to be extendable to the case of arbitrary anisotropy with some additional computational effort. Thus it is ideally suited for calculation of the waveforms expected in ultrasonic *point–source/point–receiver* measurements and in near field acoustic emission signals. It is this procedure which will be followed here.

In the following section we derive analytic expressions for the transformed displacement response to a step point load acting on the surface of a transversely isotropic plate and discuss the extensions necessary for the treatment of other sources. The numerical inversion of the transform by the method outlined above is discussed in Sect. III. In Sect. IV we present comparisons of the numerically calculated responses with calculations by means of Generalized Rays (assuming isotropic symmetry), and with experimentally determined responses in a single crystal plate specimen of zinc. We conclude with a discussion of the prospects for extending this method to materials of more arbitrary anisotropy.

III. Double transform of plate response

Consider the slab of thickness $2h = H$ pictured in Fig. 1. We imagine an excitation consisting of a point unit vertical step force $\mathbf{F}(t) = H(t)\,\hat{e}_z$ acting on an initially quiescent system, though generalization to other time dependencies, loading positions, directions and distributions is not difficult. The formal elastodynamic boundary–value, initial–value problem seeks the solution $\mathbf{u}(\mathbf{r}, t)$ of the following partial differential equation

$$c_{ijkl}\, u_{k,lj} \;=\; \rho \frac{\partial^2 u_i}{\partial t^2} \tag{4}$$

with quiescent intial conditions and with boundary conditions given by

$$\begin{aligned} c_{3jkl}\, u_{k,l} \;&=\; F_j\, \delta(x)\delta(y) \qquad \text{at} \quad z = +h \\ \text{and} \qquad & \qquad\qquad\qquad\qquad\qquad\qquad\qquad\qquad (5) \\ c_{3jkl}\, u_{k,l} \;&=\; 0 \qquad\qquad\qquad\quad \text{at} \quad z = -h \;. \end{aligned}$$

Upon performing a single temporal and a double spatial, Fourier transform on u

$$U_i(k_x, k_y, \omega, z) \;=\; \int\int\int u_i(x,y,z,t)\,\exp\{\imath(k_x x + k_y y - \omega t)\}\,dx\,dy\,dt \quad , \tag{6}$$

we find that the PDE reduces to a set of coupled ordinary differential equations. When the material is transversely isotropic with its axis of symmetry oriented normal to the plate surface, we may, without loss of generality, assume that k_y vanishes, and construct the following ODE's, where a prime signifies a derivative with respect to the z–coordinate

$$\begin{aligned} -c_{1111}\,k^2\,U_1 \;+\; c_{1313}\,U_1'' \;-\; \imath k\,[c_{1133}+c_{1331}]\,U_3' \;&=\; -\rho\,\omega^2\,U_1 \\ -c_{3131}\,k^2\,U_3 \;+\; c_{3333}\,U_3'' \;-\; \imath k\,[c_{3131}+c_{3311}]\,U_1' \;&=\; -\rho\,\omega^2\,U_3 \quad , \end{aligned} \tag{7}$$

in which U_2 decouples. General symmetry constraints amongst the elastic moduli tell us further that $c_{1313} = c_{3131} = c_{3113} = c_{1331}$ and $c_{1133} = c_{3311}$.

If one seeks solutions of the form $U_i\,\exp(\imath\alpha z)$, one recovers an algebraic problem:

$$[\,\mathbf{Q}\,]\{\mathbf{U}\} \;=\; \{\mathbf{0}\} \qquad \text{or,}$$

$$\begin{bmatrix} \rho\omega^2 - c_{1111}k^2 - c_{1313}\alpha^2 & k\alpha(c_{1133}+c_{1331}) \\ k\alpha(c_{1133}+c_{1331}) & \rho\omega^2 - c_{3131}k^2 - c_{3333}\alpha^2 \end{bmatrix} \begin{Bmatrix} U_1 \\ U_3 \end{Bmatrix} \;=\; \begin{Bmatrix} 0 \\ 0 \end{Bmatrix} \quad , \tag{8}$$

for which the characteristic equation $\det[\mathbf{Q}] = 0$ is, at fixed ω and k, a quadratic for α^2. We label the two distinct solutions of this quadratic by the subscript a which takes on the values of 1 or 2. Each value of a is associated with two related solutions, $\pm\alpha_a$, each of which is associated with an eigenvector, labeled as $\{U_\pm^a\}$. Rather than labeling the related solutions by the sign of α_a, it is convenient instead to characterize the solutions as *symmetric* (even) and *antisymmetric* (odd). One therefore takes linear combinations of the solutions associated with $\pm\alpha_a$ and forms the solutions

$$\begin{aligned} \{U^{a,e}(z)\} \;&=\; 1/2\,[\{U_+^a\}\exp(\imath\alpha_a z) + \{U_-^a\}\exp(-\imath\alpha_a z)\,] \\ &=\; \begin{Bmatrix} -\imath k\alpha_a(c_{1133}+c_{1331})\sin\alpha_a z \\ (\rho\omega^2 - c_{1111}k^2 - c_{1313}\alpha_a^2)\cos\alpha_a z \end{Bmatrix} \end{aligned} \tag{9}$$

and

$$\begin{aligned} \{U^{a,o}(z)\} \;&=\; 1/2\imath\,[\{U_+^a\}\exp(\imath\alpha_a z) - \{U_-^a\}\exp(-\imath\alpha_a z)\,] \\ &=\; \begin{Bmatrix} \imath k\alpha_a(c_{1133}+c_{1331})\cos\alpha_a z \\ (\rho\omega^2 - c_{1111}k^2 - c_{1313}\alpha_a^2)\sin\alpha_a z \end{Bmatrix} \quad . \end{aligned} \tag{10}$$

The general solution of the ordinary differential equation (Eq. (7) is an arbitrary linear combination of $\{U^{1,o}(z)\}$, $\{U^{1,e}(z)\}$, $\{U^{2,o}(z)\}$, and $\{U^{2,e}(z)\}$. That is

$$\{U\} \;=\; \sum\sum A^{a,\sigma}\,\{U^{a,\sigma}\} \quad , \tag{11}$$

where the sums are over $a = 1, 2$ and $\sigma = e, o$. Invocation of the boundary conditions allows one to determine the coefficients A of the linear combination. The transformed boundary conditions are, at the upper surface

$$c_{3311}(-\imath k)\, U_1 \;+\; c_{3333}\, U_3' \,|_{z=+h} \;=\; \frac{F}{\imath\omega}$$

and (12)

$$c_{1313} U_1' \;-\; \imath k c_{1313}\, U_3 \,|_{z=+h} \;=\; 0$$

At the lower surface of the plate $(z = -h)$ both these expressions vanish.

In principle, the resulting system of equations for the A's is 4×4, however the use of even and odd solutions rather than upgoing and downgoing solutions uncouples this 4×4 system to give two distinct 2×2 systems.

For the even modes one finds

$$\sum A^{ae} \left[c_{3311} \left(-k^2 \alpha_a\right) \left(c_{1133} + c_{1331}\right) \sin \alpha_a h \right.$$
$$\left. - \alpha_a c_{3333} \left(\rho\omega^2 - c_{1111} k^2 - c_{1313} \alpha_a^2\right) \sin \alpha h \right] \;=\; \frac{F}{2\imath\omega} \qquad (13)$$

and

$$\imath k \sum A^{ae} \left[c_{1313} \alpha_a^2 \left(c_{1133} + c_{1331}\right) \cos \alpha_a h \right.$$
$$\left. - c_{1331} \left(\rho\omega^2 - c_{1111} k^2 - c_{1313} \alpha_a^2\right) \cos \alpha h \right] \;=\; 0 \;, \qquad (14)$$

where the sums are over $a = 1, 2$. For the odd modes one finds

$$\sum A^{ao} \left[c_{3311} \left(k^2 \alpha_a\right) \left(c_{1133} + c_{1331}\right) \cos \alpha_a h \right.$$
$$\left. + \alpha_a c_{3333} \left(\rho\omega^2 - c_{1111} k^2 - c_{1313} \alpha_a^2\right) \cos \alpha h \right] \;=\; \frac{F}{2\imath\omega} \qquad (15)$$

and

$$\imath k \sum A^{ao} \left[c_{1313} \alpha_a^2 \left(c_{1133} + c_{1331}\right) \sin \alpha_a h \right.$$
$$\left. + c_{1331} \left(\rho\omega^2 - c_{1111} k^2 - c_{1313} \alpha_a^2\right) \sin \alpha h \right] \;=\; 0 \;. \qquad (16)$$

For a fixed value of ω and k one may determine the two thickness direction wave numbers α_a by solving the quadratic $\det[\mathbf{Q}] = 0$, determine the associated transformed displacement fields from Eqs. (9–11), and determine the coefficients A from the 2×2 systems of Eqs. (13–16). This completes the determination of the transformed displacement field responses. At $z = -h$, the transformed normal response is

$$U_3|_{z=-h} \;=\; \sum A^{ae} \left(\rho\omega^2 - c_{1111} k^2 - c_{1313} \alpha_a^2\right) \cos \alpha_a h$$
$$- \sum A^{ao} \left(\rho\omega^2 - c_{1111} k^2 - c_{1313} \alpha_a^2\right) \sin \alpha_a h \qquad (17)$$

At $z = +h$, the transformed response is

$$U_3 \,|_{z=+h} \;=\; \sum A^{ae} \left(\rho\omega^2 - c_{1111} k^2 - c_{1313} \alpha_a^2\right) \cos \alpha_a h$$
$$+ \sum A^{ao} \left(\rho\omega^2 - c_{1111} k^2 - c_{1313} \alpha_a^2\right) \sin \alpha_a h \;. \qquad (18)$$

The response at a receiver location (x, y), located at a distance $r = \sqrt{(x^2 + y^2)}$ from the point of application of the force is then given by the inverse triple transform:

$$u_3(x, y, z = \pm h, t) = (2\pi)^{-3} \int\int\int U_3(k_x, k_y, \omega, z = \pm h) \exp\{-\imath(k_x x + k_y y - \omega t)\}\, dk_x\, dk_y\, d\omega \quad . \tag{19}$$

Using the assumed transverse isotropy, one may recognize that U_3 is a function only of the magnitude of k and hence one can perform the integration over the direction of k analytically. One is left with the following inverse double Fourier–Hankel transform

$$u_3(r, z = \pm h, t) = (2\pi)^{-2} \int_{-\infty}^{+\infty} \int_0^{\infty} U_3(k, \omega, z = \pm h)\, J_0(kr) \exp(\imath\omega t)\, k\, dk\, d\omega \quad , \tag{20}$$

where J_0 is the Bessel function of first kind, zeroth order. Except for the relatively greater complexity of the expressions for U, this double inverse transform is identical to that obtained for the response of an isotropic slab (Vasudevan and Mal, 1985; Weaver and Sachse, 1988; Weaver, *et al.*, 1989).

The above analysis has described the method for the generation of doubly transformed displacement responses to normal surface loads. The method is, however, of greater generality and may be used to calculate responses to more arbitrary loadings. The right side of Eqs. (13)–(16) are essentially the transformed applied surface tractions, which could be generalized to loads other than normal loads. Buried sources would be slightly more complicated, the ODE (Eq. (7)) acquiring inhomogeneous forces, functions of z. Their solution would not, however, be difficult. Nayfeh and Kim (1993) have discussed doubly transformed responses to line loads in anisotropic media. Van der Hijden (1987) has formulated the procedures for the calculations of the transformed responses to point loads in arbitrarily layered anisotropic media.

The response to some of these other loadings is implicit in the present calculation. For example, the displacement response to a pair of horizontal double forces may be obtained as described in the following paragraph.

The displacement response in the radial direction to a vertical impulse may be shown to be

$$u_r(r, z = \pm h, t) = (2\pi)^{-2} \int\int U_1(k, \omega, z = \pm h)\, J_1(kr) \exp(\imath\omega t)\, k\, dk\, d\omega \quad , \tag{21}$$

where U_1 is obtained from Eqs. (9)–(16) as was U_3. Symmetry arguments may be used to show that the response in the θ direction vanishes. The in–plane (two–dimensional) divergence of the in–plane displacement field may then be formally constructed from

$$\nabla_{2d} \cdot (u_r\, \mathbf{e}_r) = (2\pi)^{-2} \int\int U_1(k, \omega, z = \pm h)\, (1/r)\, d[rJ_1(kr)]/dr \exp(\imath\omega t)\, k\, dk\, d\omega \tag{22}$$

$$= (2\pi)^{-2} \int\int U_1(k, \omega, z = \pm h)\, J_0(kr) \exp(\imath\omega t)\, k^2\, dk\, d\omega \quad . \tag{23}$$

While measurements of in plane divergence responses to normal surface loads are rarely, if ever, made, the reciprocal measurement of a normal surface displacement response to an in–plane dilation precisely corresponds to a common case in which laser generated thermoelastic sources generate ultrasound which is detected by sensors of normal surface motion. Thus, by reciprocity, Eq. (23) corresponds to an important *PS/PR* testing configuration.

The effect of a finite aperture receiver may be incorporated into Eqs. (20) or (23) by the insertion of a factor corresponding to the Hankel transform of the receiver sensitivity into the integrand. This has been demonstrated for the isotropic case (Duprey, 1993; Weaver and Sachse, 1993).

The principal interest of the present communication is in a proposed method for the evaluation of integrals such as those appearing in Eqs. (20), (21) or (23). We therefore do not concern ourselves further with the calculation of the integrand in the general case, but only with the integral. We choose to address Eq. (20).

Evaluation of one of the two integrals appearing in Eqs. (20), (21) or (23) may, as discussed in the Introduction, be effected by contour integration and the Cauchy residue theorem. That procedure requires the location of the poles, the roots of the dispersion relations for the guided waves of the plate. Alternatively one might attempt an algebraically cumbersome semi-analytical evaluation of the response by writing it as a ray sum. See, for example, the work of Knopoff (1958) or Ceranoglu and Pao (1981) for discussions of this approach in an isotropic plate.

Here we follow the algebraically less cumbersome, but computationally more demanding numerical evaluation of the double integral expressed by Eq. (20). We judge it expedient to carry out the integration in ω by means of an FFT algorithm. The numerical integration may be done in a variety of ways. It is most important to recognize that the k–integration along the real k axis passes arbitrarily close to a finite number of discrete poles at the real roots $k(\omega)$ of the guided mode dispersion relation for the plate. A reliable numerical algorithm for the navigation of these poles is, in principle, possible. However, in the spirit of constructing an algebraically simple, albeit computationally intensive method, it is arguably more appropriate to avoid the need for such programming. Mal and co-workers (Xu and Mal, 1985; Kundu and Mal, 1985; Lih and Mal, 1992) have treated the difficulty by including dissipation in their constitutive relations $c_{ijkl}(\omega)$. For real, non–zero ω this moves the poles off the real k axis. The consequent high attenuations at high frequencies have also limited the high frequencies in their responses, thereby allowing truncation of the inverse Fourier transform at moderately low frequencies. By also limiting the low–frequency content of their excitations, the pole at $\omega = 0$ is eliminated.

In this paper we follow an alternative scheme in which the Fourier transform is generalized by $\omega \rightarrow \omega_r - \imath\delta$ where δ is small and positive. While δ may, if desired, be allowed to have a dependence upon ω_r as one would if one were to make one's excursions into the complex plane only in the vicinity of the poles, the choice of a constant δ preserves the applicability of the FFT algorithm for the final ω inversion. With a constant, positive δ, it is a simple matter to show that Eq. (20) is exactly equivalent to

$$u_3(r, z = \pm h, t) \;=\; \exp(\delta t)\,(2\pi)^{-2} \int_{-\infty}^{+\infty} \int_0^{\infty} U_3\,(k, \omega_r - \imath\delta, z = \pm h)\, J_0(kr)\, \exp(\imath\omega_r t)\, k\, dk\, d\omega_r \quad (24)$$

The integrand is a non–singular function of the real variables ω_r and k. It may now be integrated numerically without ambiguity.

IV. Double Numerical Inverse Transform

The computational burden associated with the performance of the double integral appearing in Eq. (24) is not prohibitive. Issues of efficiency are therefore not critical. Inasmuch, however, as we imagine ultimate extension of the technique to the triple integrals required for responses in slabs of

arbitrary elastic symmetry, we do expect issues of efficiency to be ultimately relevant. We therefore consider them here.

The integration of Eq. (24) is performed first with respect to k at fixed ω_r, and then with respect to ω_r by an FFT algorithm. Upon choosing a temporal resolution Δt, and a range in time T, one concludes that the frequency resolution $\Delta\omega$ can be no more coarse than $\Delta\omega = 2\pi/T$. We choose $\Delta\omega = 2\pi/\nu T$ with $\nu \geq 1$ chosen to be an integer power of 2. The maximum unaliased frequency is $\omega_{max} = \pi/\Delta t$. Thus the number of independent frequencies for which the inverse Hankel transform must be evaluated and summed for the inverse Fourier transform is $\nu N/2$. For ease in implementing the FFT, we choose the number of points in the time record, $N = T/\Delta t$, to be a power of 2.

It is important when evaluating the integration with respect to k to anticipate the rate at which the integrand is likely to vary and the consequent requirements on the spacing Δk in the k–integration. The integrand of Eq. (21) has variation with k due to more than one cause. At moderate distances, when r is less than a few times the thickness $2h$, the oscillation resulting from the factor J_0 is fairly slow so that the variations in U are dominated by other causes. For large r, it is evident that the required spacings in k will be constrained due to the factor J_0 by an inequality such as $\Delta k < 1/r$.

The poles in U at the roots of the dispersion relation also contribute to rapid variations in the integrand. For a small imaginary frequency shift δ, the poles in U are very sharp, leading to the requirement that the spacing Δk in the k–integration be small. Thus there is an advantage to choosing large δ. On the other hand, a large δ will lead to large numerical noise at late times. Hence, there is some optimal choice for δ. The pole for branch 'b' is located at $k_b(\omega) \approx k_b(w_r) - k_b'(\omega_r)\imath\delta$ which lies a distance $\delta|k_b'(w_r)| = \delta/|v_g|$ from the real k axis. Here v_g is the group velocity of the branch at frequency w_r. Thus, one may anticipate that the requirement on Δk for a correct evaluation of the integral in the vicinity of the pole is something like $\Delta k < \delta/v$ where v is the group velocity of a typical guided wave mode.

One also anticipates oscillatory variations in $U(k)$ at fixed ω_r related to the presence of factors such as $\exp\{\imath\alpha_a(k,\omega)h\}$ in the expressions for U. At most points in k this factor varies with k on a scale of $1/h$. The exponent is, however, especially sensitive to variations in k near the cutoff values of k where $d\alpha_a/dk$ diverges with a square root singularity. After some algebra, one concludes with a constraint of the form $\Delta k < (h)^{-1}\,(\delta/\omega_r)^{1/2}$ which is important only in the vicinity of those few points for which $d\alpha_a/dk$ diverges. In isotropic materials, these are the points where α_a vanishes. In an arbitrary material, these are points with group velocity in the $(x$-$y)$–plane; one would therefore anticipate that they are important only in the case that source and receiver are on the same side of the plate.

In Fig. 2 is a plot of $\Im(kU_3)$ versus k for different values of δ. Note the existence of some of the anticipated scales of variation with k. The sharp behavior near the poles is evident in the limit of small δ. At larger δ there remains a smooth variation on the scale of $1/h$, comparable to the spacing between the poles. As Fig. 3 illustrates, the rapid variations versus k, anticipated to occur at the points where $d\alpha_a/dk$ diverges, are observed at $k \approx 22$ and ≈ 45.

In order to estimate an optimal value for the imaginary frequency shift δ we need to determine the value of δ for which a large Δk is tolerable because maximal Δk will correspond to a minimal computation time. As described above, we expect Δk to be chiefly constrained by δ/v. This reasoning would lead one to choose large values of δ. Such large values will lead, however, to severe constraints on integration accuracy, because errors will be multiplied by

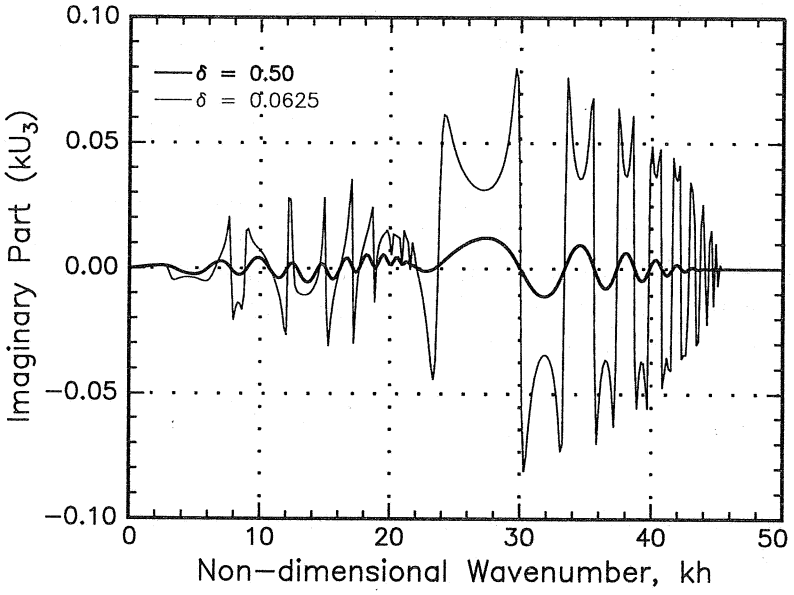

Figure 2: The behavior of $\Im\{kU_3\}$ versus kh at $\omega = 35.54, z = -h$ for a small and large values of the imaginary part of the frequency δ. The units are those described at the end of Sect. 4.

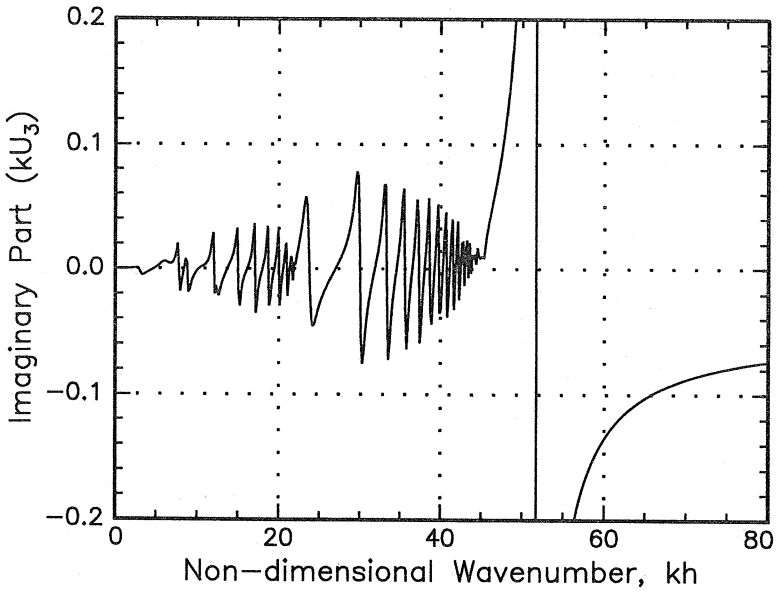

Figure 3: The behavior of $\Im\{kU_3\}$ versus kh at $\omega = 35.54, \delta = 0.0025$ and for $z = +h$. Note the surface acoustic wave pole at $k \simeq 52$ and the slow convergence as $k \to \infty$.

$\exp\{\delta T\}$. If we seek an absolute error in the computed displacements u which is less than ϵ, then the absolute error in the double integral appearing in Eq. (24) at time T must be less than $\epsilon\,(2\pi)^2\,\exp(-\delta T)$. This corresponds to an absolute error in each point ω of the inverse Hankel transform

$$v(\omega) \;=\; \int_0^\infty U_3\,(k, \omega_r - \imath\delta, z = \pm h)\,J_0(kr)\,k\,dk \quad , \tag{25}$$

which must be less than $\varepsilon\,(2\pi)^2\,\exp(-\delta T)/\omega_{max}$. If the integral appearing in Eq. (25) is evaluated using Simpson's rule (Press, *et al.*, 1989), it has a discretization error which scales with the fourth power of (Δk), $A(\Delta k/[\delta/v])^4$ where A is an unimportant scaling factor. Assuming that the discretization error dominates the error in evaluations of Eq. (25), one concludes that Δk required for the specified accuracy is determined from

$$A\left\{\frac{\Delta k}{[\delta/v]}\right\}^4 \;<\; \frac{\varepsilon(2\pi)^2\exp(-\delta T)}{\omega_{max}} \tag{26}$$

By solving Eq. (26) for Δk and differentiating with respect to δ, the maximal value for Δk is then found at $\delta = 4/T$.

As this argument depends upon the assumption that δ is small, the conclusion follows only for sufficiently large T. For moderate r and T, Δk is chiefly constrained by $1/h$. Thus the optimal value for δ is merely whatever δ makes the constraints equal, that is, $1/h \approx \delta/v$. Unfortunately this argument is not quantitatively precise and in practice we find the optimal value of δ operationally. We find optimal values of δ of the order of $2/T$. Complete theoretical understanding of these issues awaits further work.

The integral appearing in Eq. (25) is evaluated by a succession of calls to a double precision complex Simpson's rule integrator adapted from the routine QSIMP in *Numerical Recipes* (Press, *et al.*, 1986) with an relative error bound of one part in 10^6. A more sophisticated Romberg integration scheme was not found to increase efficiency.

Mal and co-workers (Xu and Mal, 1985; Lih and Mal, 1992) have developed an integration method for integrals such as that appearing in Eq. (25) in which Δk varies with k adaptively and in which the need for the constraint $\Delta k < 1/r$ is not present because the integrand without the factor J_0 is fit locally to a polynomial in k and the local integration of the oscillatory factor times the polynomial can be done exactly. This procedure is well–suited for large distances r for which the chief constraint on Δk would be $1/r$, but it is less indicated in the present case in which r is small. The adaptive variation method is not pursued here, but it is arguably more efficient than the use of uniform spacings even at small r. As Fig. (2) illustrates, the scale over which U varies does vary with k, most notably in the vicinity of the points where $\partial\alpha/\partial k$ diverges.

The integral appearing in Eq. (25) runs to infinite k. Evaluation of this improper integral is, therefore, problematic. As seen from Fig. 2, however, the integrand for the case that the receiver is on the side opposite from the source converges rapidly for k greater than some characteristic value of the order of ω_r/c_{saw}, where c_{saw} is the speed of the surface wave. A numerical evaluation of this integral may then safely be truncated at a value of k equal to k_{max} somewhat larger than ω_r/c_{saw}.

It is clear from Fig. 3, that on the top surface, when k is equal to ω_r/c_{saw}, there is a large peak, corresponding to the surface wave pole. For k larger than ω_r/c_{saw} the integrand asymptotes to a constant value. Therefore a truncation is not appropriate in this case. The integration converges only by virtue of the gently diminishing oscillations in the Bessel function

J_0. At $r = 0$ the integral does not converge at all, corresponding to the $1/r$ singularity at a point force on a half space. In order to compute this integral numerically we have chosen to evaluate the integral from the point k_{max} to ∞ by means of an asymptotic expression.

Consider the integral $I = \int_{k_{max}}^{\infty} A(k)\, J_0(kr)\, dk$ where $A(k) = kU_3(k)$ is close to its asymptotic value for all $k \geq k_{max}$. We expand the Bessel function asymptotically to obtain

$$(2/\pi r)^{1/2} \int A(k)\,(k)^{-1/2} [\cos(kr - \pi/4) + \sin(kr - \pi/4)/8kr - 9\cos(kr - \pi/4)/128k^2r^2]\, dk \quad (27)$$

By defining the quantities

$$\zeta \equiv \frac{k}{k_{max}}, \quad a(\zeta) \equiv \frac{A(k)}{\sqrt{\zeta}}, \quad b(\zeta) \equiv \frac{a(\zeta)}{\zeta}, \quad c(\zeta) \equiv \frac{a(\zeta)}{\zeta^2} \quad \text{and} \quad x \equiv k_{max} r \gg 1 \qquad (28)$$

Eq. (24) can be rewritten to obtain

$$k_{max} \left(\frac{2}{2\pi x}\right)^{1/2} \int_1^{\infty} a(\zeta)\cos(\zeta x - \pi/4) + b(\zeta)\sin(\zeta x - \pi/4)/8x - 9\, c(\zeta)\cos(\zeta x - \pi/4)/128x^2]\, d\zeta \quad (29)$$

This integral can now be evaluated for asymptotically large values of x. We find

$$\begin{aligned} I \sim\ & k_{max} \left(\frac{2}{\pi x}\right)^{1/2} [-a(1)\sin(x - \pi/4)/x - a'(1)\cos(x - \pi/4)/x^2 + a''(1)\sin(x - \pi/4)/x^3 \\ & + \left(\frac{1}{8}\right) \{b(1)\cos(x - \pi/4)/x^2 - b'(1)\sin(x - \pi/4)/x^3\} \\ & + \left(\frac{9}{128}\right) c(1)\sin(x - \pi/4)/x^3] \ , \end{aligned} \qquad (30)$$

where the primes indicate derivatives with respect to ζ. This expression is added to the Simpson's rule evaluation of the integral from zero to k_{max}. Its accuracy is checked by investigating the invariance of the final result under changes of k_{max}.

The response $u(t)$ is given by an inverse Fourier transform on v. That is

$$\begin{aligned} u(t) &= \frac{\exp(\delta t)}{4\pi^2} \int_{-\infty}^{+\infty} v(w_r - \imath\delta)\, \exp\{\imath\omega t\}\, d\omega \\ &= 2\Re \left[\frac{\exp(\delta t)}{4\pi^2} \int_0^{\infty} v(\omega_r - \imath\delta) \exp\{\imath\omega t\}\, d\omega\right] \ , \end{aligned} \qquad (31)$$

where $\Re$ indicates the real part of the expression. We evaluate the integral, however, by means of a discrete sum on v_n, where v_n is defined by

$$v_n = v((n + 1/2)\Delta\omega - \imath\delta) \qquad \text{for} \quad n = 0, 1, 2, \ldots \left(\frac{\nu N}{2} - 1\right) \ . \qquad (32)$$

The final determination of u is found in the form

$$u(t)|_{t=m\Delta t} = 2\Re \left[\exp\{\delta t + \imath\Delta\omega t/2\} \frac{\Delta\omega}{4\pi^2} \sum v_n \exp\left\{\frac{2\imath\pi nm}{\nu N}\right\} f(\omega_r)\Big|_{\omega_r = (n+1/2)\Delta\omega}\right] \ , \qquad (33)$$

where f is a low–pass filter function that brings the summand smoothly to zero at ω_{max} in order to avoid Gibbs oscillations at the ray arrival times. The sum over n is from zero to $\nu N/2 - 1$. By padding the array v with an additional $\nu N/2$ zeros, however, and extending the sum to νN terms, the sum becomes identical in form to that of a discrete Fourier Transform. It may be computed efficiently by an FFT algorithm.

The sum is a good approximation to the integral appearing Eq. (31) only if the points of the integrand are sufficiently closely sampled in the sum. If we insist that there be at least ν points per cycle of the kernel $\exp\{\imath\omega t\}$ of the integrand, we conclude that $\Delta\omega$ must be smaller than $2\pi/\nu t$ for all t of interest, i.e. $\Delta\omega = 2\pi/\nu T$. This provides an alternative meaning for the computation parameter ν, as the number of points summed in the inverse Fourier Transform per cycle of its kernel. Only the first N elements of the resulting νN element array u_m are reported, corresponding to times from zero to T.

The parameter $\nu \geq 1$ permits trading accuracy and computational burden. Large values for ν corresponding to a fine resolution in ω imply a better approximation between the sum appearing in Eq. (30) and the integral appearing in Eq. (28). The total computational effort very nearly scales with ν, however, and computations at large ν can therefore be prohibitively slow. In the results we present below, ν has been taken to equal 4. Larger values lead only to slight changes which are indistinguishable on the plots presented here. On the other hand, $\nu = 1$ leads to obvious errors, of the order of a couple of percent.

The evaluation of U and the integration of U with respect to k was conducted with 16–byte complex arithmetic. The FFT was summed with 8–byte complex arithmetic. A unit step force (i.e. $F = 1$) was used and units such that $h = \rho = c_{3333} = 1$ were used. Thus the resulting displacements are in units of $F/c_{3333}h$ and are given as a function of time in normalized time units of h/c_L where c_L is defined as the speed $\sqrt{c_{3333}/\rho}$ of a longitudinal wave along the axis of symmetry through the plate thickness. Computational times varied with the desired accuracy and desired time resolution; typical calculations required a few minutes on a workstation.

V. Results and comparison with experiment

To investigate the accuracy of the present method we have calculated the response of an isotropic slab and numerically compared it to the response obtained by generalized ray theory. We have considered the case $c_{ijkl} = \lambda\delta_{ij}\delta_{kl} + \mu(\delta_{ik}\delta_{jl} + \delta_{il}\delta_{jk})$ with $\lambda = 2\mu$ corresponding to a Poisson's ratio of $1/3$ and a ratio of longitudinal to shear wave speeds of 2. Fig. 4 shows the response at epicenter ($z = -h$, $r = 0$) calculated by the present scheme using parameters $T = 8(h/c_L)$, $\delta = 2/T$, and $\nu = 4$. The results of a generalized ray calculation at epicenter (c.f. Knopoff (1958)) in which the response is given by an explicit algebraic expression are superposed. As in our previous work (Weaver and Sachse, 1988; Weaver, *et al.*, 1989), the slight differences cannot be descerned on the scale of the plot. The difference between the calculations is shown in the inset in which it can be seen that, except near the ray arrival times at which the very high frequency limitations of the present technique are most evident, typical errors are less than 10^{-5}. As anticipated, they increase at later times.

Results from the present calculation for a receiver on the same side ($z = +h$) as the source and at a distance of $r = 2h = H$ are shown in Fig. 5, superposed upon the results of a generalized ray calculation calculated using the code developed by Hsu (1985). The maximum descrepancy is less than 10^{-5} except in the vicinity of the arrival times. Much of the error has a characteristic

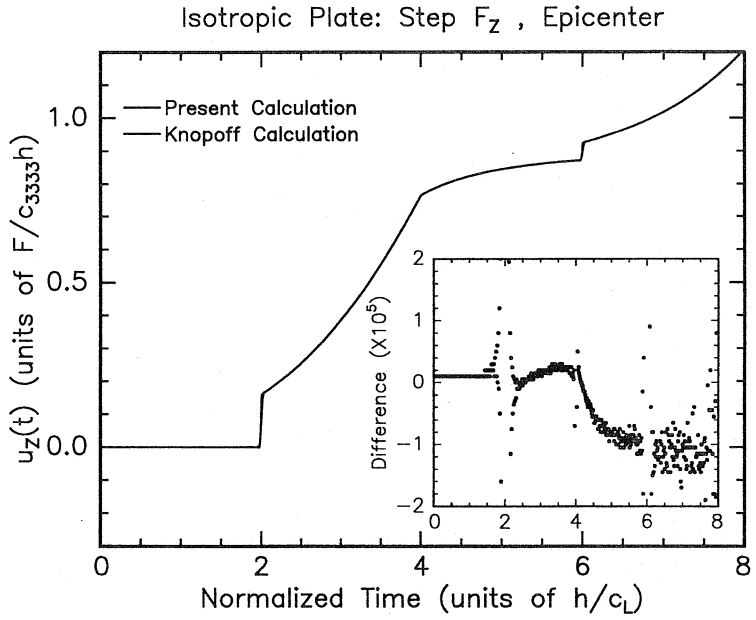

Figure 4: The displacement response at epicenter in an isotropic plate as calculated by the present method is indistinguishable from the explicit formula given by Knopoff (1958). The insert shows the difference between these two approaches on an expanded scale.

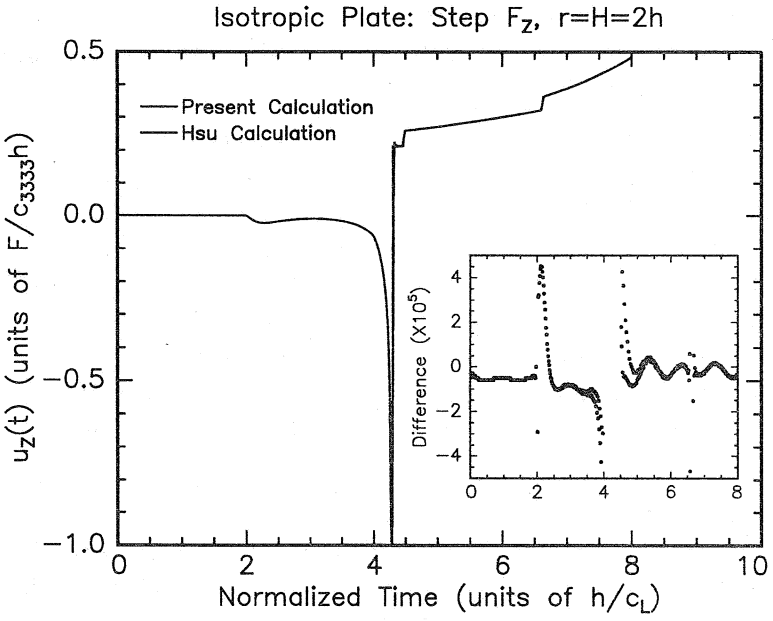

Figure 5: The response at a distance $r = 2h$ from the source on the same side as the detector in an isotropic slab is calculated by the present method and by generalized rays. The difference is shown in the insert. Note in particular the significant Rayleigh wave arrival.

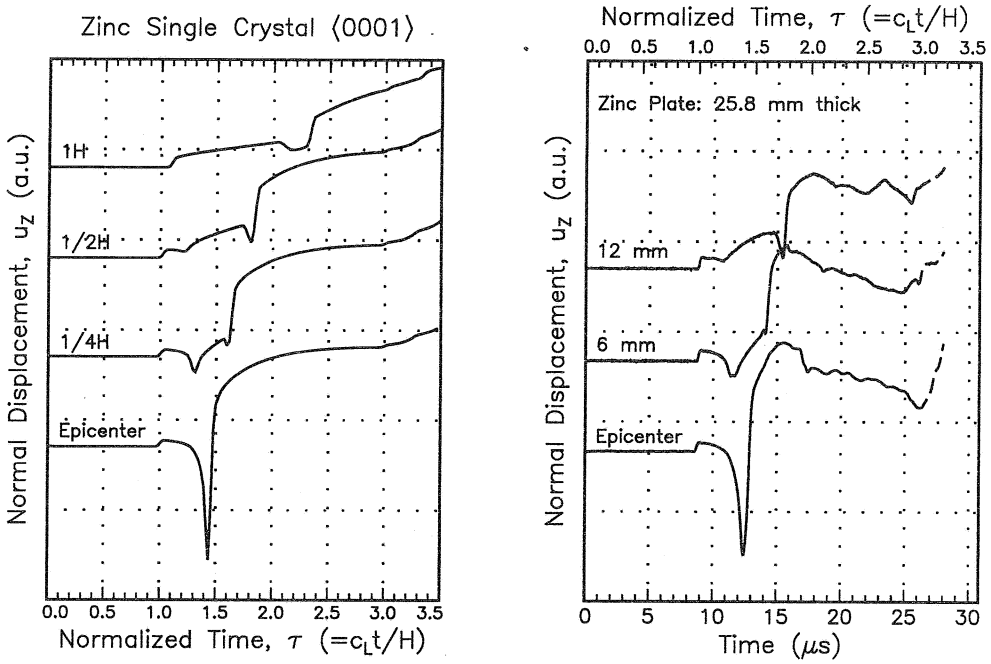

Figure 6: Responses at several positions on the side of the plate opposite from the source. (a) Calculated responses. (b) Measured results. (Note: 6.5 mm $\simeq \frac{1}{4}H$; 13 mm $\simeq \frac{1}{2}H$)

time scale and appears non stochastic, indicating that the descrepancies are not the result of round–off error or finite precision in the integrations, but rather the result of some small systematic error in the code. They are not removed by increasing the parameter ν, nor by demanding that the k–integrations be carried out to an accuracy of one part in 10^7, nor do they change upon adjusting the nominally arbitrary parameter k_{max}.

We also apply the present algorithm to the case of a zinc single crystal plate whose elastic symmetry axis is aligned normal to the surface. We choose the following values for the ratios of the elastic moduli: $c_{1111}/c_{3333} = 2.6021$, $c_{1313}/c_{3333} = 0.6147$, and $c_{1133}/c_{3333} = 0.8339$. In Fig. 6 we show a set of responses at $z = -h$, calculated for a series of different source/receiver separations. Results from measurements in zinc, reported elsewhere (Kim and Sachse, 1993), are also shown. The agreement is good, the differences at late times being ascribable to side wall reflections in the experiment and to low frequency rolloff in the ultrasonic receiver electronics. In particular one should note the strong (ideally infinite) response at the arrival of the focused conical point rays. The behaviour of these curves has been discussed at length elsewhere (Kim and Sachse, 1993).

The computed and measured responses on the same side as the source (at $z = +h$) at a distance $r = 2h$ are shown in Fig. 7. Note in particular, the strong surface wave arrival in the computed waveform, at $t = r/c_{saw} = 2.91$ in units of h/c_L or 12.54 μs and also the conical point wave reflected off the bottom of the plate specimen, arriving at $t = 30.5$ μs. The first signal is at $t = 1.24$ in units of h/c_L or 5.45 μs, corresponding to the propagation of the very fast longitudinal wave in the direction normal to the symmetry axis. The arrival of the surface wave in the measured normal displacement waveform is in excellent agreement with that computed. The surface wave amplitude is significantly smaller than that of the computed signal and there is noticeable spreading of the trailing edge of this signal. The measured signal exhibits other differences from the ideal computed case after ~ 20 μs. The differences are likely the result of material damping, the arrivals of reflected signals from the boundaries of the specimen, and the low–frequency roll–off in the

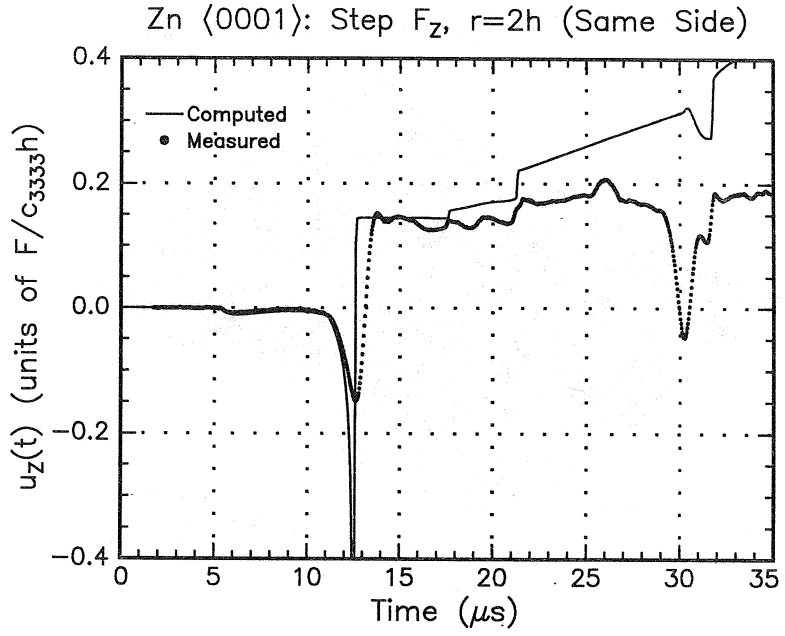

Figure 7: Computed and measured responses in zinc at $r = H = 2h$ on the same side of the plate as the source. The measured waveform has been shifted horizontally by a constant (corresponding to the pre–trigger time) to bring the first arrival signals into coincidence and scaled vertically by a constant (corresponding to the source strength and charge amplifier gain) to bring the amplitude after the surface wave arrival into agreement.

receiver electronics.

In previous work we have shown that by stacking a large number of signals measured or calculated at adjacent source/receiver configurations, one obtains a *scan image* which represents the detailed spatial and temporal characteristics of the elastic wave field in a material that can be directly related to the material's anisotropy and macrostructure (Every and Sachse, 1991). Fig. 8 shows a synthetic scan image consisting of a stack of 101 waveforms similar to those of Fig. 6, corresponding to a range of receiver positions between epicenter and 20 mm off–epicenter in a 25.8 mm thick single crystal plate of zinc whose c–axis was aligned with the normal to the plate. This image clearly shows the wave arrivals of the various bulk wave modes and, in particular, their amplitude evolution. Of particular recent interest has been the extraordinarily high amplitude of the epicentral conical ray, which is the result of the focusing of the quasi–transverse wave modes toward the symmetry direction. This is related to the phenomenon of *external conical refraction* (Kim, *et al.*, 1993b).

VI. Discussion and Conclusions

We have shown the applicability of a conceptually simple, albeit computationally demanding, procedure for the calculation for wave responses in a transversely isotropic thick plate by means of double numerical inverse transforms. This method is particularly well suited for calculations of responses in the near field of layered structures, and is easily generalized for calculation of responses in viscoelastic media, and to include the effects of finite aperture sources and receivers. The singularities of the integrand are eliminated by the introduction of a small, but non–zero, imaginary part to the frequency. Except for issues of numerical accuracy, the procedure is, in principle, exact. By

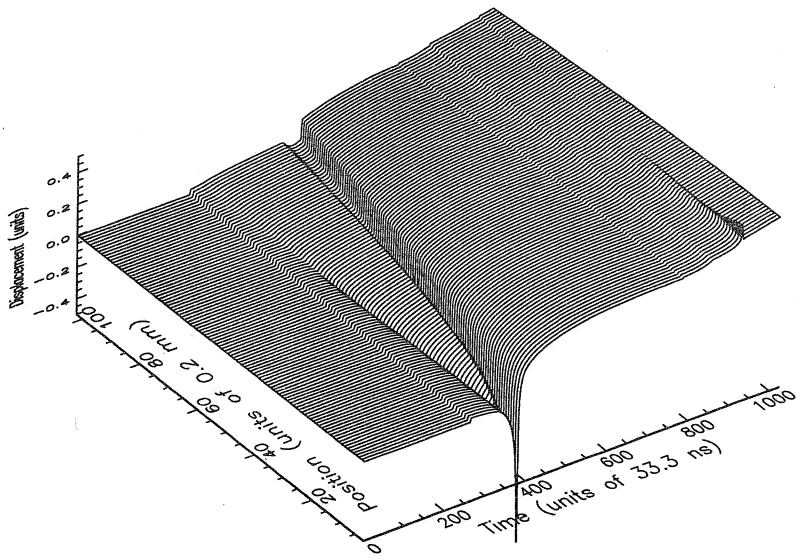

Figure 8: Synthetic *scan image* of a single crystal plate specimen of zinc. The receiver position ranges from epicenter to 20 mm off–epicenter on the opposite side of the plate as the source.

including another numerical transform, the method can be generalized to calculate the responses in materials of more general symmetry.

Generalization to materials of more arbitrary anisotropy is of particular importance for future work. The consequent additional numerical inverse transform can be expected to significantly increase the computational burden. If the accuracies and time resolution achieved here were to be retained in the non–axisymmetric case, one estimates the computational burden in the generalization to be greater by a factor of about 10^4. For such applications, it may therefore prove worthwhile to seek additional methods for the k–integration which are more efficient than the simple Simpson's rule used here.

As an illustration, we have used this approach to calculate synthetic plate responses which could be compared to those measured in a single crystal specimen of zinc. Expected application of these calculations include *point-source/point–receiver* ultrasonics, quantitative acoustic emission measurements and seismology.

VII. Acknowledgements

This work has been supported in part by the MRL Program of the National Science Foundation under Award No. DMR–9121654. RLW was also supported, in part, by NSF grant MSS91–14360. WS and KYK were also supported in part by the Office of Naval Research (Physical Acoustics Program).

References

Bedding, R. J. and Willis, J. R., 1980, "The elastodynamics Green's tensor for a half space with an embedding anisotropic layer", *Wave Motion*, **2**(1),, 51–62.

Bouchon, M. and Aki, K., 1977, "Discrete wavenumber representation of seismic–source wave fields", *Bull. Seism. Soc. of Am.*, **67**, 259–277.

Castagnede, B., Kim, K. Y., Sachse, W. and Thompson, M. O., 1991, "Determination of the elastic constants of anisotropic materials using laser-generated ultrasonic signals", *J. Appl. Phys.*, **70**(1), 150–157.

Ceranoglu, A. N. and Pao, Y. H., 1981, "Propagation of Elastic Pulses and Acoustic Emission in a Plate", *ASME J. Appl. Mech.*, **48**, 125–147.

Chang, C. and Sun, C. T., 1988, "Acoustic emissions and transient elastic waves in an orthotropic laminate plate", *Composite Sci. Tech.*, **33**, 213–236.

Duprey, K., 1993, *Attenuation Recovery in Viscoelastic Plates including the Effects of Finite Aperture Transducers* M. S. Dissertation, Cornell University, Ithaca, NY.

Every, A. G. and Sachse, W., 1990, "Determination of the elastic constants of anisotropic solids from acoustic wave group velocity measurements", *Physical Review B*, **42**(13), 8196–8205.

Every, A. G. and Sachse, W., 1991, "Imaging of laser-generated ultrasonic waves in silicon", *Physical Review B*, **44**(13), 6689–6699.

Every, A. G., Sachse, W., Kim, K. Y. and Niu, L., 1991, "Determination of elastic constants of anisotropic solids from group velocity data", in *Review of Progress in Quantitative Nondestructive Evaluation*, **10B**, D. O. Thompson and D. E. Chimenti, Eds., Plenum Press, New York (1991), pp. 1663–1668.

Every, A. G. and Kim, K. Y., 1993, "Time domain dynamic response functions of elastically anisotropic solids", Submitted for publication, *J. Acoust. Soc. Am.*

Hsu, N. N., 1985, "Dynamic Green's Functions of an Infinite Plate – A Computer Program", NBSIR 85–3234, National Bureau of Standards, Gaithersburg, MD.

Kim, K. Y. and Sachse, W., 1993, "Direct determination of group velocity surfaces in a cuspidal region in zinc", MSC Report #7582, Materials Science Center, Cornell University, Ithaca, NY. In Press: *J. Appl. Phys.*

Kim, K. Y., Sachse, W. and Hsieh, P., 1989, "Quantitative study of fracture by acoustic emission from cracks", in *Advances in Fracture Research*, Vol. 5, K. Salama, K. Ravi-chandar, D. M. R. Taplin and P. R. Rao, Eds., Pergamon Press, New York, pp. 3185-3196.

Kim, K. Y., Sachse W. and Every, A. G., 1993a, "On the determination of sound speeds in cubic crystals and isotropic media using a broadband ultrasonic point–source/point–receiver method", *J. Acoust. Soc. Am.*, **93**(3), 1393–1406.

Kim, K. Y., Every, A. G., and Sachse, W., 1993b,"Focusing of acoustic energy at the conical point in zinc", *Phys. Rev. Letters*, **70**, 3443–3446.

Knopoff, L., 1958, "Surface Motions of a Thick Plate", *J. Appl. Phys.*, **24**, 661–670.

Kundu, T. and Mal, A. K., 1985, "Elastic waves in a multilayered solid due to a dislocation source", *Wave Motion*, **7**, 459–471.

Lih, S. S. and Mal, A. K., 1992, "Elastodynamic response of unidirectional composite laminates to concentrated loads", *J. Appl. Mechanics*, **59**, 878–886; 887–894.

Nayfeh, A. and Chimenti, D., 1989, "Free wave propagation in plates of general anisotropic media", *J. Appl. Mech.*, **56**, 881–888.

Nayfeh, A. and Kim, Y.–Y., 1993, "Wave propagation in anisotropic media due to internal transient line loads". Paper read at the ASME–AMD Summer Meeting, Charlottesville, VA (June 1993), in *Meet'N'93, Abstracts*, p. 504.

Niu, L., 1992, *The Determination of the Elastic Constants of Composite Materials from Ultrasonic Group Velocity Data*, Ph. D. Dissertation, Cornell University, Ithaca, NY.

Pao, Y. H., and Gajewski, R., 1977, "The Generalized Ray Theory and Transient Responses of Layered Elastic Solids", Chapt. 6 in *Physical Acoustics*, Vol. XIII, W. P. Mason and R. N. Thurston, Eds., Academic Press, New York, pp. 183–265.

Payton, R. G., 1983, *Elastic Wave Propagation in Transversely Isotropic Media*, Martinus Nijhoff, Hague.

Pekeris, C. L., 1955, "The seismic surface pulse", *Proc. Natl. Acad. Sci.*, **41**, 469–480; 629–638.

Press, W. H., Flannery, B. P., Teukolsky, S. A. and Vetterling, W. T., 1986, *Numerical Recipes*, Cambridge University Press, Cambridge, UK.

Sachse, W. and Kim, K. Y., 1986, "Point-source/point-receiver materials testing", in *Review of Quantitative Nondestructive Evaluation*, **6A**, D. O. Thompson and D. E. Chimenti, Eds., Plenum Press, New York, pp. 311–320. Also: 1987a, in *Ultrasonic Materials Characterization II*, J. Boussière, J. P. Monchalin, C. O. Ruud and R. E. Green, Eds., Plenum Press, New York, pp. 707–715.

Sachse, W. and Kim, K. Y., 1987b, "Quantitative acoustic emission and failure mechanics of composite materials", *Ultrasonics*, **25**, 195–203.

Sachse, W., Castagnede, B., Grabec, I., Kim, K. Y. and Weaver, R. L., 1990a, "Recent developments in quantitative ultrasonic NDE of composites", *Ultrasonics*, **28**, 97–104.

Sachse, W., Every, A. G., and Weaver, R. L., 1991, "Interpretation of ultrasonic *PS/PR* amplitude data", in *Review of Progress in Quantitative Nondestructive Evaluation*, **10A**, D. O. Thompson and D. E. Chimenti, Eds., Plenum Press, New York, pp. 129–136.

Santosa F. and Pao, Y. H., 1989, "Transient axially asymetric response of an elastic plate", *Wave Motion*, **11**, 271–295.

Scruby, C. B., 1985, "Quantitative acoustic emission techniques", Chapt. 4, in *Research Techniques in Nondestructive Testing*, Vol. VIII, R. S. Sharpe, Ed., Academic Press, London, pp. 141-210.

Van der Hijden, J. H. M. T., 1987, *Propagation of Transient Elastic Waves in Stratified Anisotropic Media, Applied Mathematics and Mechanics*, **Vol. 32**, North–Holland, Amsterdam.

Vasudevan N. and Mal, A. K., 1985, "Response of an elastic plate to localized transient sources", *J. Appl. Mech.*, **52**, 356–362.

Weaver, R. L. and Pao, Y. H., 1982a, "Axisymmetric waves excited by a point source in a plate", *J. Appl. Mechanics*, **49**, 821–836.

Weaver, R. L. and Pao, Y. H., 1982b, "Spectra of transient elastic waves in elastic plates", *J. Acoust. Soc. Am.*, **72**, 1933–1941.

Weaver, R. L. and Sachse, W., 1988, "Asymptotic viscoelastic rays in a thick plate", T&AM Preprint, Cornell University, Ithaca, NY. In Press: *Journal of Applied Mechanics.*

Weaver, R. L., Sachse, W. and Niu, L., 1989, "Transient ultrasonic waves in a viscoelastic plate; Part I. Theory; Part II. Applications to materials characterization", *J. Acoust. Soc. Am.*, **85**(6), 2255–2261; 2262–2267.

Wu, T. T. and Kuo, C.–L., 1990, "A study of acoustic emission waves in double layer composite plates", in *Progress in Acoustic Emission V*, Japanese Society for NDI, Tokyo, pp. 217–221.

Xu, P. C. and Mal, A. K., 1985, "An adaptive integration scheme for irregularly oscillating functions", *Wave Motion*, **7**, 235–243.

List of Recent TAM Reports

No.	*Authors*	*Title*	*Date*
711	Weaver, R. L.	Anderson localization in the time domain: Numerical studies of waves in two-dimensional disordered media	Apr. 1993
712	Cherukuri, H. P., and T. G. Shawki	An energy-based localization theory: Part I—Basic framework	Apr. 1993
713	Manring, N. D., and R. E. Johnson	Modeling a variable-displacement pump	June 1993
714	Birnbaum, H. K., and P. Sofronis	Hydrogen-enhanced localized plasticity—A mechanism for hydrogen-related fracture	July 1993
715	Balachandar, S., and M. R. Malik	Inviscid instability of streamwise corner flow	July 1993
716	Sofronis, P.	Linearized hydrogen elasticity	July 1993
717	Nitzsche, V. R., and K. J. Hsia	Modelling of dislocation mobility controlled brittle-to-ductile transition	July 1993
718	Hsia, K. J., and A. S. Argon	Experimental study of the mechanisms of brittle-to-ductile transition of cleavage fracture in silicon single crystals	July 1993
719	Cherukuri, H. P., and T. G. Shawki	An energy-based localization theory: Part II—Effects of the diffusion, inertia and dissipation numbers	Aug. 1993
720	Aref, H., and S. W. Jones	Chaotic motion of a solid through ideal fluid	Aug. 1993
721	Stewart, D. S.	Lectures on detonation physics: Introduction to the theory of detonation shock dynamics	Aug. 1993
722	Lawrence, C. J., and R. Mei	Long-time behavior of the drag on a body in impulsive motion	Sept. 1993
723	Mei, R., J. F. Klausner, and C. J. Lawrence	A note on the history force on a spherical bubble at finite Reynolds number	Sept. 1993
724	Qi, Q., R. E. Johnson, and J. G. Harris	A re-examination of the boundary layer attenuation and acoustic streaming accompanying plane wave propagation in a circular tube	Sept. 1993
725	Turner, J. A., and R. L. Weaver	Radiative transfer of ultrasound	Sept. 1993
726	Yogeswaren, E. K., and J. G. Harris	A model of a confocal ultrasonic inspection system for interfaces	Sept. 1993
727	Yao, J., and D. S. Stewart	On the normal detonation shock velocity–curvature relationship for materials with large activation energy	Sept. 1993
728	Qi, Q.	Attenuated leaky Rayleigh waves	Oct. 1993
729	Sofronis, P., and H. K. Birnbaum	Mechanics of hydrogen–dislocation–impurity interactions: Part I—Increasing shear modulus	Oct. 1993
730	Hsia, K. J., Z. Suo, and W. Yang	Cleavage due to dislocation confinement in layered materials	Oct. 1993
731	Acharya, A., and T. G. Shawki	A second-deformation-gradient theory of plasticity	Oct. 1993
732	Michaleris, P., D. A. Tortorelli, and C. A. Vidal	Tangent operators and design sensitivity formulations for transient nonlinear coupled problems with applications to elasto-plasticity	Nov. 1993
733	Michaleris, P., D. A. Tortorelli, and C. A. Vidal	Analysis and optimization of weakly coupled thermo-elasto-plastic systems with applications to weldment design	Nov. 1993
734	Ford, D. K., and D. S. Stewart	Probabilistic modeling of propellant beds exposed to strong stimulus	Nov. 1993
735	Mei, R., R. J. Adrian, and T. J. Hanratty	Particle dispersion in isotropic turbulence under the influence of non-Stokesian drag and gravitational settling	Nov. 1993
736	Dey, N., D. F. Socie, and K. J. Hsia	Static and cyclic fatigue failure at high temperature in ceramics containing grain boundary viscous phase: Part I — Experiments	Nov. 1993
737	Dey, N., D. F. Socie, and K. J. Hsia	Static and cyclic fatigue failure at high temperature in ceramics containing grain boundary viscous phase: Part II — Modelling	Nov. 1993
738	Turner, J. A., and R. L. Weaver	Radiative transfer and multiple scattering of diffuse ultrasound in polycrystalline media	Nov. 1993
739	Qi, Q., and R. E. Johnson	Resin flows through a porous fiber collection in pultrusion processing	Dec. 1993
740	Weaver, R. L., W. Sachse, and K. Y. Kim	Transient elastic waves in a transversely isotropic plate	Dec. 1993